



HAL
open science

Interventional radiology virtual simulator for liver biopsy

Pierre-Frédéric Villard, Franck P. Vidal, Llyr Ap Cenydd, Richard Holbrey, S. Pisharody, Sheena Johnson, Andy Bulpitt, Nigel W. John, Fernando Bello, Derek A. Gould

► **To cite this version:**

Pierre-Frédéric Villard, Franck P. Vidal, Llyr Ap Cenydd, Richard Holbrey, S. Pisharody, et al.. Interventional radiology virtual simulator for liver biopsy. International Journal of Computer Assisted Radiology and Surgery, 2013, pp.1-13. 10.1007/s11548-013-0929-0 . hal-00849184

HAL Id: hal-00849184

<https://inria.hal.science/hal-00849184>

Submitted on 30 Jul 2013

HAL is a multi-disciplinary open access archive for the deposit and dissemination of scientific research documents, whether they are published or not. The documents may come from teaching and research institutions in France or abroad, or from public or private research centers.

L'archive ouverte pluridisciplinaire **HAL**, est destinée au dépôt et à la diffusion de documents scientifiques de niveau recherche, publiés ou non, émanant des établissements d'enseignement et de recherche français ou étrangers, des laboratoires publics ou privés.

Interventional Radiology Virtual Simulator for Liver Biopsy

P.F. Villard · F.P. Vidal · L. ap Cenydd ·
R. Holbrey · S. Pisharody · S. Johnson · A.
Bulpitt · N.W. John · F. Bello · D. Gould

Received: 25 January 2013 / Accepted: 5 July 2013

Abstract *Purpose:* Training in Interventional Radiology currently uses the apprenticeship model, where clinical and technical skills of invasive procedures are learnt during practice in patients. This apprenticeship training method is increasingly limited by regulatory restrictions on working hours, concerns over patient risk through trainees' inexperience, and the variable exposure to case mix and emergencies during training. To address this, we have developed a computer-based simulation of visceral needle puncture procedures.

Methods: A real-time framework has been built that includes: segmentation, physically-based modelling, haptics rendering, pseudo-ultrasound generation and the concept of a physical mannequin. It is the result of a close collaboration between different universities, involving computer scientists, clinicians, clinical engineers and occupational psychologists.

Results: The technical implementation of the framework is a robust and real-time simulation environment combining a physical platform and an immersive computerized virtual environment. The face, content and construct validation has

P.F. Villard
LORIA, University of Lorraine, France.
E-mail: Pierrefrederic.Villard@loria.fr

P.F. Villard · F. Bello
Imperial College London, UK

F.P. Vidal · L. ap Cenydd · N.W. John
School of Computer Science, Bangor University, UK.

R. Holbrey · A. Bulpitt
School of Computing, University of Leeds, UK.

S. Pisharody
Department of Computer Science, University of Hull.

S. Johnson
Manchester Business School, University of Manchester, UK.

D. Gould
Royal Liverpool Hospital, UK.

been previously assessed, showing the reliability and effectiveness of this framework, as well as its potential for teaching visceral needle puncture.

Conclusion: A simulator for ultrasound-guided liver-biopsy has been developed. It includes functionalities and metrics extracted from cognitive task analysis. This framework can be useful during training, particularly given the known difficulties in gaining significant practice of core skills in patients.

Keywords Biomedical computing · Image segmentation · Simulation · Virtual reality

1 Introduction

1.1 Problem Statement and Motivation

Interventional radiology (IR) procedures rely on an operator's sense of touch and the use of medical imaging to guide a needle towards a specific, anatomical or pathological structure. Where necessary, a biopsy may be obtained from the targeted structure, or the needle can act as a conduit to deliver a guide-wire and catheter for further diagnostic and therapeutic intervention. These procedures are guided throughout by radiological imaging (fluoroscopy, ultrasound, computerised tomography (CT)). This paper focuses on the core skills of ultrasound-guided needle puncture, illustrated by the liver biopsy task. This procedure uses hand-eye co-ordination of ultrasound imaging and needle manipulation to target a liver mass for biopsy diagnosis.

The skills for these challenging tasks are currently acquired during an apprenticeship in patients. First, a needle is inserted through a small skin incision that eliminates the high forces required for skin puncture, which can interfere with accurate initial targeting. The needle is then progressively advanced through tissues visualised by the ultrasound. The ultrasound (US) screen shows deformation as tissue planes are punctured and then crossed by the needle. On approaching vascular structures, the needle may transmit a periodic pulsation to the operator. A tumour target will often feel very firm, with moderate to high resistance to needle passage into the tumour tissue, just before a biopsy is taken.

The challenges of this apprenticeship are: reducing time to train due to work time directives (Europe and USA); risk to patients from errors during training; missed opportunity costs from extended procedure times due to training 'on the job'; skills learnt are dependent on the case mix available at the training institution.

The aim of this research article is to describe the design of a comprehensive, ultrasound guided needle insertion simulator that incorporates physiological motion of respiration, haptics, tool manipulation and dynamic ultrasound.

1.2 State of the Art

A simulator for an interventional radiology procedure must correctly replicate the conditions wherein an operator uses relevant cognitive and technical skills to

accurately align an US probe and its image with the inserted needle and the intended anatomical target or organ (e.g. the site of a liver biopsy). Three kinds of technologies have successively appeared to design such training platforms: i) non computer-based simulators (i.e. physical mannequins), ii) computer-based simulators with generic patients and iii) patient-specific computer-based simulators.

“Low-tech” home grown alternatives have been developed by hospitals to teach ultrasound guided needle puncture [21,9]. The Manchester Royal Infirmary, for example, makes use of a home-built phantom model. The training consists of inserting the needle tip into fabricated blood vessels using images provided by a real US machine for guidance.

In [6], the acoustic properties of materials are estimated from the Hounsfield units in the CT data. Ultrasound images are then simulated using a simplified physics model. The method is relatively fast, but does not allow real-time computations. A similar approach is used on graphics processing unit (GPU) in [24]. Real-time performance is achieved (10-15 FPS), but this is not sufficient for a VR application with haptics rendering, where the frequency needs to be at least 1000 Hz to accommodate the high sensitivity of human touch. An alternative approach is to add visual properties of US images (shadowing, speckle, reflection) to the CT data [27,19]. Current US simulation methods focused exclusively on producing high levels of realism are computationally expensive and therefore unable to take internal organ motions into account, even when GPU programming is deployed. Our goal, on the other hand, is to teach hand-eye coordination with respect to the US plane, the needle and a tumour deforming as a result of respiratory motion.

Whilst low-tech alternatives may offer a good trade-off between safety and cost, the ability of such alternatives to properly recreate the required degree of variability in terms of: i) different patient anatomy, ii) customizable physiological behavior (respiration) iii) variable soft-tissue characteristics and iv) different target location, is very limited.

Ultrasound guided needle puncture simulators using a virtual environment (VE) can provide a more realistic experience than low-tech phantoms [27,19,18]. A full virtual environment can capture and recreate features such as different patient morphologies, complex physiological behaviors and elaborated performance metrics.

VE-based simulators may be divided into two categories: i) those using three-dimensional (3D) models designed by computer graphics artists and ii) those based on patient specific imaging data. Patient based simulators present an opportunity for closer correlation between a simulated task and the real task performed in a patient. A recent review of the state of the art [32] presents a list of such platforms. In our work, geometrical patient data is extracted from medical imaging studies (commonly CT or magnetic resonance imaging (MRI)) and used to build a 3D virtual environment with which the user interacts using his/her natural sense of touch via haptic devices. An example of such a prototype is presented in [5], which simulates brain tumor surgery and has been tested in 22 hospitals. Validation by experts suggested that the simulator is a reasonably realistic model of reality (face validation), though user performance metrics have not been extracted. The training potential of the simulator might be improved through implementing additional features that will increase the level of realism, such as a physical mannequin [23], haptic devices and physical palpation [4]. Metrics that report a user’s performance and progression of learning are a critical and innovative feature of computer-based

simulation technologies. These are computed in [7], but lack validation by experts with rigorous statistical tests (content validation) or validation by experts that the simulator appears to be reasonable to model reality (face validation). Finally, recent commercial simulators are beginning to include patient-specific procedures with metrics and validation [33], though without organ intrinsic behaviour such as respiration.

1.3 Contribution

The main deficiencies of the previous related simulators cited above can be summarized as the lack of:

1. Physical mannequin for early patient manipulation (not found in the literature).
2. Dynamic geometries, i.e. deformation due to palpation or needle insertion and breathing motion (static geometries are used in [27, 19]).
3. Dynamic ultrasound generation (unconvincing US generation from CT scans in [8, 27, 19] or use of pre-recorded real ultrasound data).
4. Tissue-specific force feedback during the needle insertion (a foam mannequin is used in [19]).
5. Clinical evaluation (no clinical validation of [8, 19, 18] or at an early stage and without clinical evidence of the benefit of the simulator [27]).
6. Various validated metrics to assess user performance.

One of the key contributions of this paper is precisely to gather all these components and to demonstrate how they can be integrated together in a single real-time simulator.

The design and development of a targeted liver biopsy simulation platform was based on a detailed cognitive task analysis (CTA), which identified the functionalities and metrics required using procedural videos and interviews with field experts. The CTA data are publicly available via the project website.¹

An exhaustive validation study of the simulator presented here has been published in [14], but without the comprehensive details of development, fabrication, architecture and integration of the technology used, which is now described within this second paper.

We obtained ethical approvals for the use of anonymous, patient-based medical imaging data and sensor based identification of instrument-tissue interactions.

2 Methods

This section presents in detail the main technical components that have been addressed to build the simulator. The work presented has been carried out by a six University partnership (CRaIVE consortium: Collaborators in Radiological Interventional Virtual Environments¹) brought together to address issues in training in IR. Our strategy was to divide the simulator into two separate workstations. The first (Workstation one - WS1) uses a mannequin to locate the incision and

¹ <http://www.craive.org.uk> (last accessed: 16/04/2013)

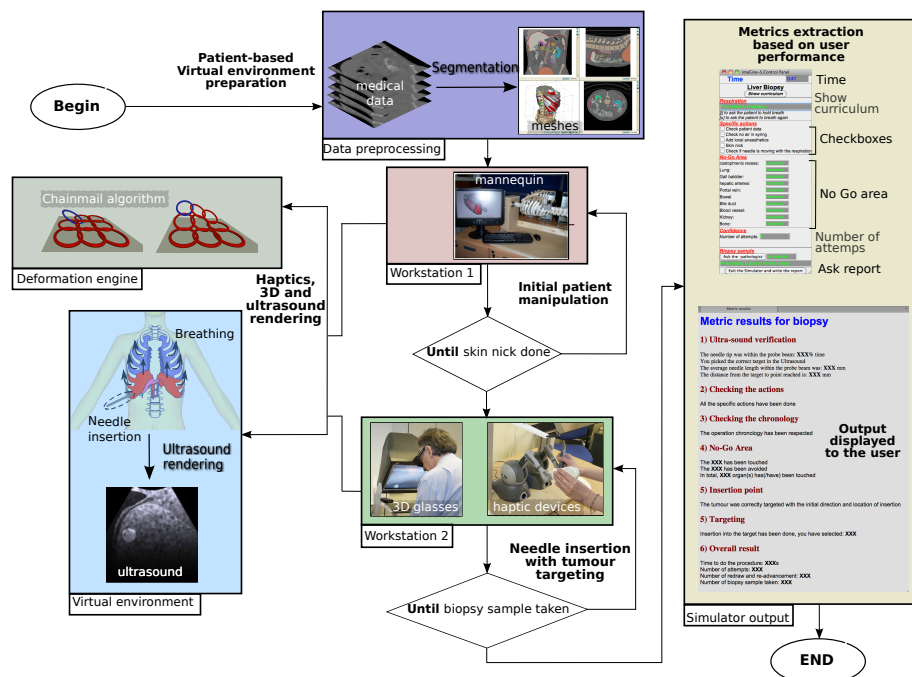


Fig. 1 General overview of the simulator showing all the components from the preprocessing step to the simulator output. It also shows the two workstations.

insertion point for the operation, thus recreating the physical contact with the patient (palpation, anatomical landmarks, skin interface, etc.). Once this location is defined, the user moves to the second workstation (Workstation two - WS2), which comprises a virtual environment with two haptic devices, one to perform needle insertion, the other to use an ultrasound probe for needle guidance. We chose to use a virtual environment in workstation two to support anatomical variability, a range of pathologies and patient specificity. The general workflow of our simulator is presented in Fig. 1.

The information gathered through CTA resulted in a VE that is customised to patient specific data, including modelling and deformation of organ motion, haptics rendering, and the concept of a physical mannequin. Simulation metrics identified through CTA were used to evaluate relevant steps of the trainee's performance. In order to assess the face, content and construct validity of the simulator, a validation study was conducted where interventional radiologists with different levels of expertise completed a liver biopsy procedure on the simulator [14]. A comparison of performance (using the metrics included in the simulator) by expertise level allowed the assessment of simulator validity. More specifically, it was shown that experienced interventional radiologists perform better on the simulator than less experienced ones [14].

Acceptable area	liver - 1 fat tissue - 2 skin - 3 diaphragm - 4
No-go area	lungs - 5 gall bladder - 6 hepatic arteries - 7 portal vein - 8 bowel - 9 bile ducts - 10 blood vessel - 11 kidneys - 12 bones - 13 costophrenic recess - 14

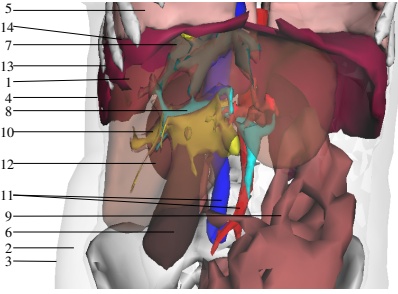


Fig. 2 Anatomical structures that have been segmented following the CTA, divided into acceptable and no-go areas

2.1 Critical Anatomical Structures

The CTA data provided key anatomical and physiological properties encountered during the liver biopsy task. Anatomical structures were graded to provide metrics that determine whether needle insertion is into ‘acceptable’ or ‘no-go’ areas (structures at risk from inadvertent puncture) as listed on Figure 2. Many of these are not currently represented in commercial simulators, even though some of the them are of interest during a liver biopsy IR procedure. Some of the key ‘no-go’ anatomical structures identified and unique to our simulator are discussed below:

Costophrenic recess: During deep inhalation, the region between the diaphragm and the ribs opens slightly so that the lungs can expand into this space. It is not desirable to penetrate the membrane where this lung expansion occurs due to the risk of injury to the lung. The membrane and recess, however, are not usually visible in medical images and thus cannot be segmented using existing tools. In our breathing model, this region is defined as a narrow wedge-shaped strip within the rib-cage.

Intercostal (‘between ribs’) neurovascular bundles: The position and motion of the ribs are significant, in particular the intercostal needle approach commences with palpation of the ribs to identify a suitable entry site (see Section 2.7). This entails avoidance of the neuro-vascular bundle (of blood vessels and nerves), which lies just below each rib, and where inadvertent puncture can produce life-threatening bleeding. Hence, the correct entry point lies immediately above a rib.

Liver ducts and vessels / gallbladder: The liver receives blood supply from the hepatic artery and portal vein via the centrally-placed porta hepatis. This also contains the common hepatic (bile) duct. In addition, just below this level lie the cystic artery and duct that connect to the gall-bladder. It is around and below this region where there is particular risk from punctured blood vessels, gallbladder or bile ducts, which may result in the release of bile or blood freely into the abdominal cavity.

2.2 Image segmentation

The image segmentation process produces a discretely labelled 3D image. Techniques can be classified according to the level of automation achieved. Fully or partially automated schemes, such as thresholding or active shape modelling, are at one extreme, whilst manually assisted segmentations are at the other. Researchers have also used rule-based approaches, such as Chi *et al* [3], who used local edge enhancement near the ribs to provide a constraint for a liver growth model. Bottger *et al* [2] used simplex meshes driven by user-selected points and image gradients to assist the segmentation of 4D heart ventricle and lung data. The output image data are typically converted into surface meshes after applying the marching cubes algorithm [17] on each label and post-processing with decimation and smoothing.

In our approach, a number of constraint-based controls are applied. The main component employed is the narrow-band level-set algorithm offered by ITK-SNAP,² in which ‘seeds’ grow within locally competing regions [35]. The narrow-band method assumes that forces generated by intensity gradients in the image can be balanced by geometric constraints depending on curvature in a local neighbourhood of points, both of the segmented object, and from other global parameters selected by the user.

Two additional constraints have been implemented by modifying the ITK-SNAP source code to create a *segmentation editor* tool. Firstly, growth data from each step of the algorithm are stored in a separate image space to limit the problem of level-set segmentation leakage (e.g. between the ribs). If a leak occurs, the operator can rewind the process and freeze the growth at a particular point by using the stored propagation history. Secondly, a surface-based constraint method has been introduced to exploit surrounding organs, which are typically easier to segment. If the user places a seed point within the object of interest, the relevant parts of meshes generated on surrounding tissues can be obtained by comparing surface normals. Data from this procedure can then be used to update the region-competition image and thus to control subsequent level-set growth.

For our purpose, bones are the most natural constraint and are relatively easy to obtain using thresholds applied on the CT data, although care is needed to avoid the aggregation of contrast-enhanced venous structures and to maintain the separation of adjacent bony ribs. A connected-components tool (using ITK [13]) was added to our editor tool to assist in the exclusion of these organs. The lungs are also relatively easy to obtain by thresholding.

In order to use the rib-cage as a general constraint, we employ the surface reconstruction method of Hoppes [12] on point data gathered from the interior of the ribs, soft ribs, etc. As the density of the data is much greater near the meshed data, it must be sub-sampled and smoothed, followed by interpolation between the ribs. For the latter, we used linear kriging. Inputting this data into Hoppes’ method then produces a 3D field, which is zero at the computed constraint location, and positive/negative to either side. In our implementation, this allows the user to adjust the position or thickness of the constraint to achieve the best possible outcome. This tool is particularly useful where the level-set method leaks into the region of rib muscle, but it is also effective for separating conjoined items such as bony ribs and spinal processes. The other organs were obtained through a

² <http://www.itksnap.org/> (last accessed: 06/01/2013)

mixture of the above mesh and morphological tools, apart from the costophrenic recess where the breathing model was used to generate point data at the maximum inhalation and exhalation positions.

The segmentation of the abdominal organs can then be constrained by the rib-cage and lung data. The smaller organs (e.g. kidney, spleen, gall-bladder) are usually more accessible, since hard edge and strong curvature constraints may be used initially and relaxed later, to give reasonable results. The liver has previously been segmented in [1], where a number of fast, automated schemes have been outlined. However, our approach is less automated and more generic, thus avoiding the need to create extensive libraries of pre-computed models for each tissue. Other arterial and venous structures were captured from contrast enhanced images at the point where they exit the liver, as impact of the biopsy needle is much more hazardous in this region.

Our experience of using these methods can be illustrated by a typical example of segmentation of the liver. This required approximately 4 hours by hand, but, by using the techniques outlined here, segmentation time was reduced to only 1.5 hours, part of which may be unsupervised.

2.3 Soft Tissue Deformation

An overview of soft tissue deformation methods [22] presents an evaluation according to three characteristics: mechanical realism, topology management, and speed of computations. Our simulation requires real time behaviour of the virtual tissues as they interact with the needle and with each other. Based on this requirement we chose the Chainmail algorithm [11] as it offers an acceptable trade-off between quality of deformation and computational complexity.

Having obtained and post-processed the virtual anatomy as described above, the simulator then consists of a 3D triangular mesh environment, facilitating dynamic ultrasound rendering. The virtual organs are not static and may undergo rigid motion or deformation, which would not be easily computed using a voxel-based environment.

To implement our soft tissue deformation model, the geometry is first re-sampled into nodes and triangles. The distance between two nodes is parameterized by three Chainmail parameters: i) the compression, which defines its minimum value; ii) the stretch, which defines its maximum distance; and iii) the shear, which adds the influence of the tangential displacement to the distance value. The initial topology changes during the simulation according to both these parameters and node displacements. When a displacement is applied to a node, it moves by the given value. Authorized boundary displacements are computed with the chainmail parameters and the displacement amplitude. When the displacement is within this boundary, the neighbour of the node does not move. When the displacement is outside, the neighbour will be affected and may propagate the motion to its own neighbours based on the same method (see Fig. 3). Practically, we use the 3D extension of the chainmail defined in [16].

In our simulator, there are two types of deformations depending on whether they are the result of applying internal or external forces. The intrinsic deformations are due to the respiration and will be explained in the next section. The external forces are the result of the needle action on the organ, and thus directly

linked to the haptic environment, which gives the positions and directions of the virtual needle. The vertices belonging to the face directly touched by the needle are computed internally in the haptic API. The variation in the needle's position as the operator drives it through the virtual skin is then applied as a displacement to this node. This feature is especially useful when the liver capsule starts to deform during insertion, as it allows the operator to locate the tip of the needle without it actually being visible on the US screen. A more detailed explanation of our chainmail implementation can be found in [29].

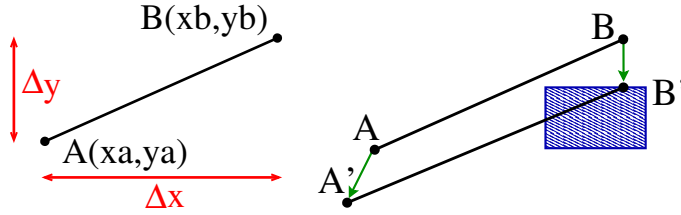


Fig. 3 Chain mail algorithm. Left: original position of A and B, right: A is moved to A' but B is not in the valid region anymore: it is moved to the nearest point of the valid region

2.4 Respiratory Motion

Simulating respiratory motion is vital to ensure a high level of realism on the simulator. Such organ motion is a very important cue for the image guidance during the needle insertion. Therefore, the virtual patient should be able to breathe or hold its breath when required. Furthermore, it should be possible to vary the type of breathing: tidal breathing, hyperventilation, diaphragmatic or thoracic breathing, etc. Hence, we chose to use a simulated online respiration model, instead of a pre-computed model such as in [25]. Fig. 4 shows how we divided the thoracic organs and the viscera into five categories: i) static rigid organs, ii) rigid organs with rotational motion, iii) rigid organs with translational motion, iv) deformable organs, and v) deformable organs with internal contraction.

According to this classification, the spine belongs to the first group. It could be considered as static if the patient lies on a bed. Moreover, all the bones except the ribs are considered to be rigid bodies as the deformations are negligible. The ribs, on the other hand, belong to the second group. Their motion is associated to rotations as described in [34]. Each rib is defined by a rotation centre and two types of rotation: one in the spine axis (as a pump handle), and a second one in the anterior-posterior axis (as a bucket handle). The rotation magnitude could vary, as well as the frequency of this kinematic movement.

The organ targeted in the procedure (tumour) belongs to the third group. In the case of liver biopsy, a 24mm diameter sphere is added to the virtual environment to represent a tumour. It has been placed in the liver just below the diaphragm. This location has been chosen by our clinical collaborators to represent a real case study. The tumour experiences a sinusoidal translation inside the liver.

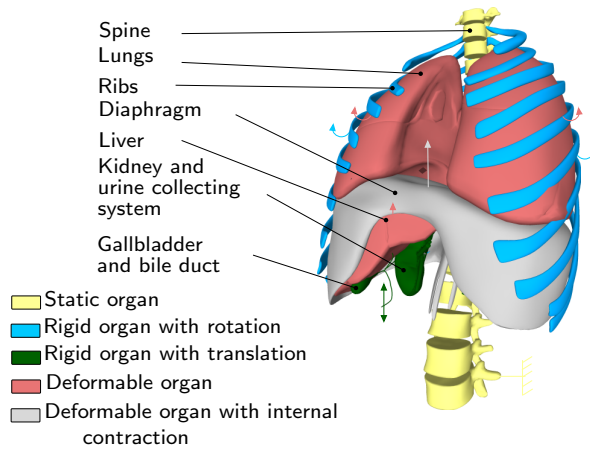


Fig. 4 Organ motion categories during respiration

Other viscera whose deformation could be neglected such as the gallbladder are included in this group. For larger organs where the deformations are noticeable, the Chainmail algorithm is used. Such organs are passive and then linked to surrounding organs that impose constraints within the Chainmail loop. This is the case of the lungs compressed by the ribcage and the diaphragm, and of the liver compressed by the diaphragm. Both lungs and liver belong to the fourth group. The diaphragm is slightly different as it is subject to internal contraction and thus belongs to the fifth group. Its deformation is also linked to a surrounding organ (ribs). To capture the complex behaviour of the diaphragm, we modelled it as a heterogeneous body composed of a rigid part (the tendon), and an elastic part (the muscle). The contraction and relaxation actions of the diaphragm muscle are modelled by a variable (amplitude and frequency) sinusoidal motion of the tendon propagated through the chainmail algorithm. A more detailed explanation of our respiratory motion model can be found in [30].

In order to ensure that the geometrical errors between reality and the simulation are minimised, the parameters of the respiration model and of the chainmail model were automatically tuned using the optimization technique described in [28], where the authors showed that it is possible to follow the liver with an error below 4.5mm.

2.5 Haptic Rendering

The simulator makes use of two modified Phantom Omni force feedback devices. The first is used to simulate the probe manipulation. There is basic collision detection and collision response with the patient's skin. Ultrasound rendering is performed based on the device position and orientation (see Section 2.6). The second Phantom device is used to simulate needle insertion. Experts acknowledge that force feedback when inserting a needle through the liver needs particular attention. Therefore, force feedback for this organ is treated differently from that of the other organs within our simulator. Forces generated by two needles (18 G

Kimal,³ 21 G Chiba⁴) during punctures of fresh porcine liver specimens (<3 hours post-slaughter) were measured using a validated sensor [15]. Ten measurements at 10 different liver sites were acquired at constant needle velocities of: 50 mm/min, 125 mm/min, 250 mm/min and 500 mm. The obtained force data was plotted against displacement and time. Various models of needle insertion can be found in the literature [10]. We have chosen an analytical model [20] based on a succession of exponential-like rises before and after liver capsule penetration, and proportional to needle insertion depth. The model was fitted to the experimental data, and used to render force feedback during needle insertion within the simulator. This model is the basis of our haptic rendering for the puncture of the liver and builds on our previous work [27].

The force feedback provided for other organs is based on Hooke's law. For a given type of tissue, a look-up table (LUT) of stiffness coefficients has been empirically defined by our medical collaborators. Force feedback for a particular tissue type is then proportional to this coefficient and the depth of penetration of the needle between two successive iterations of the haptic rendering algorithm. The change in elasticity between different tissues is based on the CT scan voxel gradient. When the needle passes from one kind of tissue to another, a rise in stiffness is felt because the tip of the needle has to perforate the surface of the underlying tissue. This boundary between tissues is determined using the norm of the CT scan voxel gradient. After the penetration of the tissue, its stiffness parameter is extracted from the LUT. In addition to these models, a lateral constraining force is applied to the needle to ensure it follows a straight line trajectory once it has been inserted through the skin, just as it would during a real procedure where it would be difficult to move the needle off its initial trajectory. The Phantom device used in the simulation to mimic the needle provides 6 degrees of freedom (DOF) in tracking, but only 3 DOF in force feedback. Hence, the force is applied just to the end point of the stylus and, because there is no torque, the stylus can be moved freely in all directions and orientation (pitch, roll and yaw). To address this deficiency, the orientation of the stylus is ignored during the puncture stage and the needle is constrained to follow a straight line, unless the needle tip remains in superficial tissues (i.e. up to 2 cm below the skin surface). This reflects the fact that during real procedures, the angle of the needle may be adjusted slightly whilst the needle tip is still located in superficial tissues, to allow the target to be successfully located, but the angle cannot be adjusted once the needle has been more deeply inserted.

2.6 Ultrasound Rendering

Trainees in IR are already familiar with the appearance and interpretation of real world ultrasound imaging. This project is therefore less concerned with training imaging interpretation, than with the technical skills of hand-eye co-ordination using visual and tactile cues. In particular, to allow deliberate practice of the technical skills to maintain and advance a needle towards a target, whilst both are kept within the ultrasound imaging plane.

³ safety fistula needle manufactured by Kimal, <http://www.kimal.co.uk/> (last accessed: 16/04/2013)

⁴ hollow needle used in IR, named after Chiba University in Japan, where it was invented.

The ultrasound renderer generates real-time, ultrasound-like images of the dynamic patient model, given the position and orientation of the virtual probe. As the main objective of the simulator is to teach hand-eye coordination, the renderer aims to reproduce the salient features of an ultrasound image, such as bone and gas shadowing, boundary reflection, attenuation and speckle. We have updated our previous work to use dynamic polygon meshes as input data instead of CT scans [27].

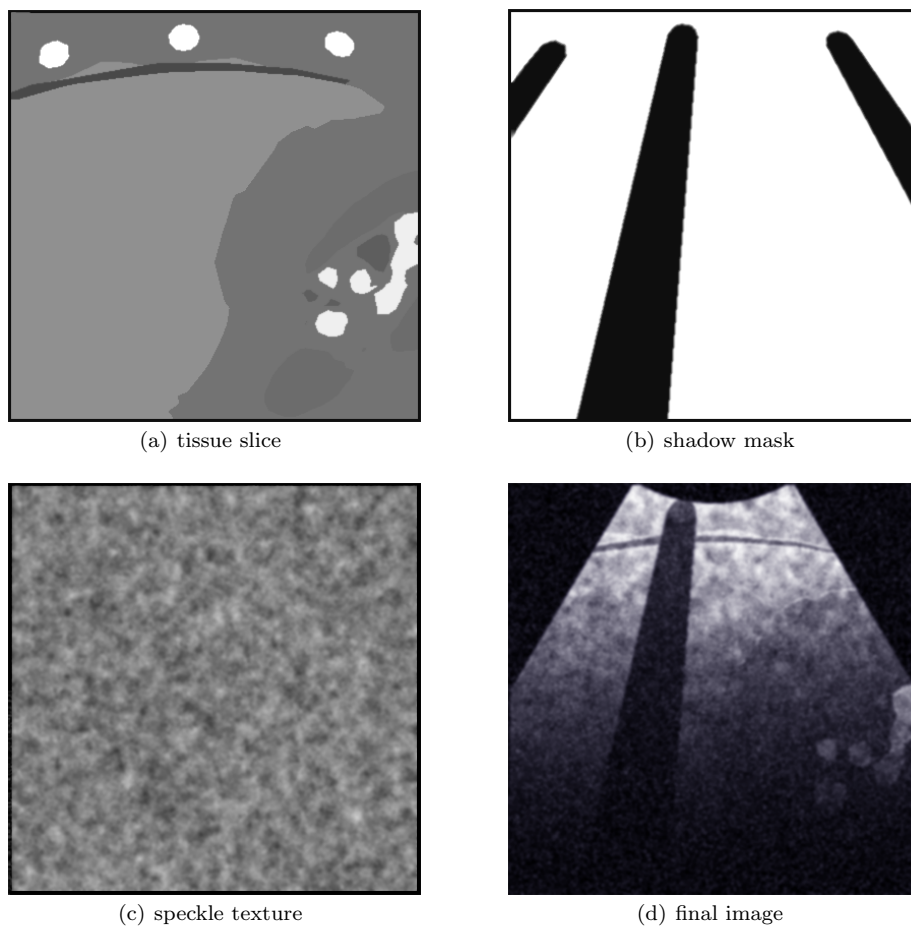


Fig. 5 Ultrasound image composition. The tissue slice (a), is combined with a calculated shadow mask (b) and speckle texture (c) to give the final composited image (d).

Three images are generated by the renderer for every frame: i) a tissue slice, ii) a shadow mask, and iii) a speckle texture. These are passed to a GLSL (OpenGL Shading Language) shader for composition, enhancement and filtering, producing the final displayed image.

The first step in our algorithm is to render a thin slice of the mesh environment, given the position and orientation of the ultrasound probe (see Fig. 5(a)). An orthographic projection gives the axis-aligned box representing the ultrasound image-plane. The horizontal and vertical clipping planes are scaled by the required ultrasound slice thickness, whereas the near clip plane is set to zero. Each specific tissue in the patient model is tagged with a corresponding Hounsfield value, which is used to shade every pixel in the mask with an appropriate brightness. While it is possible to perform this part of the rendering process on all meshes at once, any intersecting meshes in the scene will cause z-fighting artifacts in the final image. Due to the dynamic meshes used in our simulation, we chose to render objects of differing tissue types in separate rendering passes. This does result in a small reduction in performance, but produces a clean image where tissues are clearly defined.

In US imaging, hard structures like bone completely reflect the ultrasound wave, resulting in a shadow being cast behind such structures. Similarly, acoustic shadowing due to sound reflecting at gas/tissue interfaces also result in a darkening of more distal structures. This effect can be simulated by post-processing the previously rendered image slice to create a separate shadow mask (Fig. 5(b)). As each tissue is assigned a brightness based on its Hounsfield value, it is possible to identify the presence and location of bone and gas in the rendered image. Each pixel in the shadow mask is initialized to 1. The rendered tissue image is then processed with corresponding pixels in the shadow mask lying behind bone/gas structures set to a lower value.

Speckle is observed in all real ultrasound images. In our simulation, the speckle is represented by a precomputed stack of 2D isotropic images, loaded into the graphics card's memory as a 3D texture. It represents speckle voxels within the patient, and is scaled and rotated to fit the boundary of the virtual patient. Knowing the position, orientation and depth of the ultrasound probe's imaging plane, and the virtual patient's configuration, we can sample a corresponding 2D multi-planar reconstruction of speckle for the ultrasound image (see Fig. 5(c)).

Fig. 6 shows an example of the needle's appearance in our ultrasound renderer. The needle is part of the mesh environment, and is therefore rendered into the tissue image along with all the patient meshes. The needle's geometry is split into two sections: i) the shaft, which is shaded very faintly, and ii) the tip, which is made much brighter. This is an accurate representation of a real-life needle in ultrasound image. The displacement of local tissue due to needle shaft penetration is approximated by shifting the coordinates of the speckle texture sampling appropriately: the effect being a subtle displacement along the needle's shaft, with the needle tip being much easier to locate due to its brightness.

In the final rendering stage, all three generated images (tissue slice, shadow mask and speckle texture) are combined within a GLSL compositing shader. In order to render the correct sector shape for a curvilinear transducer at the chosen depth, only pixels that lie within a calculated mask are processed.

Bright reflections occur in US images at certain interfaces, such as between fat/tissue. This effect is generated in the final image by detecting and enhancing horizontal edges using a Sobel filter to compute the gradient direction. Reflections will occur when the gradient direction along the vertical axis of the image is above a given threshold. Other effects are also applied, including reducing the image brightness with increasing distance from the probe, and adjusting the image

contrast and brightness using shift/scale filters. Finally, a Gaussian filter shader is used to smooth out any pixellation or processing artefacts in the ultrasound image (see Fig. 5(d) and Fig. 6).

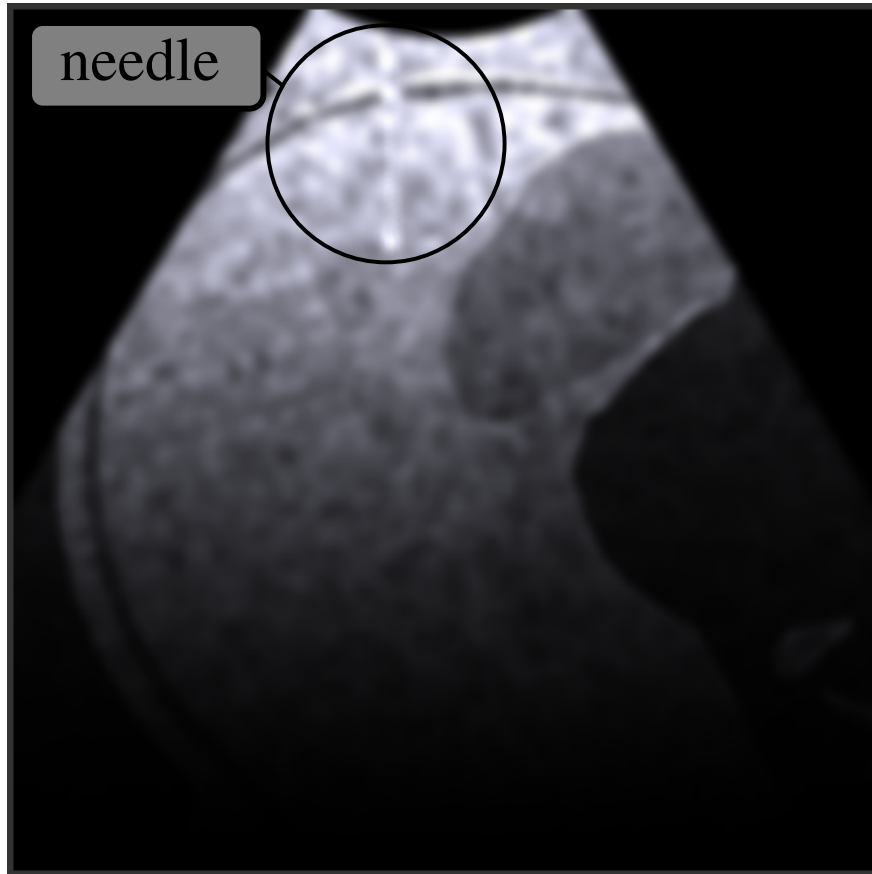


Fig. 6 Needle in rendered ultrasound image (top left)

2.7 Mannequin

With a view to improving the face validity of the simulator for training purposes, a custom-built breathing life-size torso mannequin was introduced as a first point of interaction with the system (see Fig. 7). A plastic skeleton forms the core structure of the torso, with soft foam forming the layers of fat and muscle. A silicone skin outer covering provides the look and feel of human skin. The respiration was achieved using a bespoke servo-controlled motorised rib cage. The rib cage movement simulates both the pump-handle rotation, and the bucket-handle

rotation. Parameters such as rib rotation angle and respiration frequency are adjustable through software and have been co-registered to the respiration simulation in the virtual environment. The mannequin was also co-registered to the patient-specific datasets for liver biopsy. The mannequin registration was a challenging task performed manually using rigid transformations of the skin surfaces. Lastly, a magnetically-tracked ultrasound probe co-registered to the mannequin provided simulated ultrasound rendering as described previously. The probe position registration on the mannequin uses the 3D Thin Plate Splines method [31]. Even if the registration of the real patient's anatomy with the mannequin cannot be perfect due to the rigid properties of the registration, the position of the probed can still be finely set. Moreover, the clinical validation showed the trainee is fully immersed and is not affected by the registration errors.

The ultrasound probe switches on when in contact with the skin surface. A magnetically tracked scalpel was also designed to enable the radiologist to make a skin nick to identify the point for needle insertion. A switch at the tip of the scalpel was used to activate position marking.

The mannequin was mounted on a specially designed stand to enable rotation along its spine, thereby allowing the radiologist to position the patient as required for individual procedures. A potentiometer was used to measure mannequin rotation in order to reproduce rotational movement on the patient in the virtual environment. The patient rotation and skin nick markings were passed to the second workstation to identify the needle puncture site. The physical mannequin is optional in our simulator as the skin nick can also be performed within the virtual environment.



Fig. 7 Mannequin ribcage synchronised with the virtual environment (3D meshes and ultrasound rendering). *Inset:* patient and ultrasound probe in the virtual environment

2.8 Metrics

Whilst performance metrics may be obtained by tracking devices during real procedures [26] to obtain quantities such as needle tip distance to target, distance traveled by guided needle tip, efficiency scores, quality score, item difficulty, performance index and guidance error index, such quantities may also be calculated in simulated procedures directly from the simulator input devices without any additional effort. This represents a crucial advantage of using a computer-based simulator for training as it can objectively assess the performance of each individual user, as well as follow his/her progression by recording or calculating performance metrics during the procedural simulation.

Based on interviews of subject matter experts (SMEs), various metrics were proposed to assess all the crucial steps identified in the task analysis. The identified metrics reflect the experts' judgment about the crucial steps that the trainee must do and avoid during the intervention. Several of these proposed metrics have been implemented in our simulator. They can be classified in different categories as detailed below.

The first set of metrics is composed of tick boxes. They are of two kinds. The first kind is linked to the preparations before and after the procedure. The user can confirm that various actions have been completed: "check the patient's data", "check there is no air in the syringe", "add local anaesthetics", "ensure urine drips". The second kind is done during the manipulation. The user ticks them while doing the tasks: "do the skin nick", "check if the needle is moving with the respiration", "ask the patient to hold his breath", "ask the patient to breathe again". The chronology of these tasks is also tested with a clock function integrated in the interface. The total time to perform the procedure is therefore also saved as a metric. The tick boxes are used to teach the task chronology. It is important not to omit key parts of the procedure even if they are not fully simulated as this could result in negative training and is likely to increase the omission of key steps during real procedures.

The next set of metrics is linked to the needle insertion. Each time the needle is inserted into the skin, the number of attempts is recorded, along with the location and direction of insertion. The location is then compared to the best area of insertion used by three experts to produce a performance metric. This insertion site was a surface drawn on the skin above the tenth rib. Location and direction are also compared to the local anaesthetic injection path. As the needle is inserted further, the simulator checks for proximity to surrounding organs. If a "no-go area" is touched, a warning message is displayed and the error is logged. Once the target is reached and the user activates the haptic button to trigger the biopsy, the accuracy of the position is recorded. The haptic components of the simulator representing the needle and ultrasound probe provide continuous updates of position and orientation at graphical frame rates of around 25 frames per second. As the project CTA described requirements for liver biopsy, an arbitrary target of 20 mm was placed at relevant locations and the results assessed with respect to the specified requirements. In particular, the CTA suggested that both the target and needle should be visible as much as possible in the ultrasound data, and that, ideally, the needle tip (which is acoustically brighter) should also be visible. Whether or not the needle tip is visible (but especially if not), it was strongly recommended that the full length of the needle should be visible to minimise working outside the

ultrasound beam. Bearing this in mind, the ‘beam’ in our simulation was modelled as a 40 mm wide and 4 mm thick trapezoid, whereas the needle was 150 mm in length. The metrics assessed for validation comprised time and distance quantities, which are related to the presence or absence of the target or needle (or length of the needle) within the virtual beam. The metrics included are:

1. Whether the target was hit
2. The proportion of the time (whilst the probe was active) during which the target was visible
3. The mean needle length visible within the virtual beam as averaged over each session
4. The total time over which the ultrasound probe was employed during the session
5. The number of no-go areas (as defined by the CTA) touched
6. The overall time taken
7. The distance covered by the needle tip during the session
8. The number of initial skin contacts taken to place the needle
9. The total time spent by the needle in no-go areas

3 Results

3.1 Input data

The use of real patient imaging data was agreed by the local research ethics committee. A 3D CT scan of a patient attending the Liverpool Royal Hospital (UK) was selected as a representative patient case. The pathology configuration was established to maximise pedagogical value in terms of tumor location and patient anatomy. Scan parameters were as follows: size $512 \times 512 \times 190$, and voxel dimensions $1\text{mm} \times 1\text{mm} \times 3\text{mm}$.

3.2 Integration

The algorithms previously described were implemented in C++ using the H3D⁵ framework, an API handling haptic interaction as well as graphics rendering. A major challenge was to successfully integrate the code from the four participating centres. The final simulator prototype is composed of two workstations. Workstation 1 (WS1) consists of the mannequin with the ultrasound display (see Section 2.6). Workstation 2 (WS2) is composed of a SenseGraphics 3D Immersive Workbench⁶ presenting the virtual environment in 3D, using two Phantom Omni for the haptic rendering (see Section 2.5), and the same ultrasound screen as WS1 (see Fig. 8).

The sequence of the simulation is as follows: the user is invited to scan the mannequin on WS1 and to perform the skin nick as discussed on 2.7. This location is then passed on to WS2 and displayed to show where the needle should be inserted. Once in WS2 and after inserting the needle through the first layer of fat, the user

⁵ <http://www.h3dapi.org/> (last accessed: 16/04/2013)

⁶ <http://www.sensegraphics.com/> (last accessed: 16/04/2013)

can stop the patient’s breathing and verify that the organ motion has stopped on the ultrasound screen before proceeding further. As the needle is inserted, the metrics (see 2.8) record the triangulation between the needle, the ultrasound-scanning plane and the target. Once the target is reached, the simulation ends and the quality of the operation is evaluated through the computed metrics which are displayed to the user. Ultrasound rendering is performed throughout the procedure, together with organ motion due to respiration (except during the brief interruptions or breath holds). The virtual environment is extracted and generated as described in 2.1.



Fig. 8 Integration of Workstation 1 and Workstation 2

3.3 Validation results

Following development of the simulator and implementation of its performance metrics, results of a validation study of the liver biopsy procedure were published in [14], demonstrating the reliability and effectiveness of the simulator framework described in this paper. A brief overview of the validation results is provided below.

Ethical approval was granted by the Liverpool Research Ethics Committee (UK) and participants ($n=40$) working in 3 UK hospitals with varying degrees of expertise in IR were recruited to the study. In total, fourteen consultants and twenty-six trainees completed the simulated liver biopsy procedure. The performance metrics were then investigated as differentiators between levels of expertise in Interventional Radiology. Participant scores on the performance metrics were compared between consultants and trainees, and across years of experience. Significant differences were found in the expected direction (that is, better performance was associated with increased expertise) for *Targeting*, *Probe usage time*, *Mean needle length in beam*, *Number of no-go areas touched*, *Length of session*, *Total needle distance moved*, *Number of skin contacts* and *Total time in no-go area*.

In addition to the significant differences by expertise found for the above metrics, inspection of the scores for each of the other liver biopsy performance metrics revealed a predictable pattern across experience. That is, although not all differences were statistically significant, there was a consistent pattern across all metrics showing that more experienced participants received better performance scores.

Finally, evidence for the face and content validity of the simulator was indicated with 84% of participants believing it would be useful in learning the steps of a procedure, and 81% agreeing that it would be useful for procedure rehearsal. Furthermore, 80% of participants reported that the feedback provided by the simulator was accurate. These results show that technical limitations (e.g. lack of torque force feedback to simulate the counter-force from the orientation along the insertion directions, or the use of a simplified US image rendering model) still provide a level of fidelity that is high enough for training purposes.

Feedback was sought from participants on the strengths and weaknesses. Areas identified for future improvement were the ultrasound rendering and the deformation of the organs.

4 Conclusion

This paper presents the integration, including novel components, of a simulation to train interventional radiologists. It consists of state-of-the-art features common to other recent virtual simulator models such as ultrasound and haptics rendering, physically-based deformation framework, performance metrics, physical mannequin, face validation and content validation. It also includes novel modules to reproduce real life characteristics of the procedures, such as patient breathing, ultrasound image deformation and a dynamic physical mannequin. The strength of this simulator is to train a user to anticipate an organ's intrinsic motions, visualising a moving tumour target using ultrasound. Even though the on-line ultrasound rendering is not entirely realistic, the results of the published validation study [14] suggest that it is sufficient to improve the triangulation skill, i.e. to be able to see at the same time in the ultrasound plane both the target (e.g. tumour) and the whole length of the needle within the simulated ultrasound 'beam'.

The simulator's content is aligned with a target curriculum (Royal College of Radiologists) and includes case scenarios based on patient-customised anatomical data, which can be used to train liver biopsy. Studies of the effectiveness of the simulation have been performed in collaboration with interventional clinicians and include content validation where end-user feedback was positive. Construct validity was demonstrated with experts performing significantly better than trainees on a number of performance metrics [14]. It was concluded that it is possible to measure and monitor performance using simulation, with performance metrics providing feedback on skill level in relation to specific aspects of the procedure. This should enable participants to identify those elements of a procedure they have either mastered or that requires further skill development. This is likely to be useful during training, particularly given the known difficulties in gaining significant practice of core skills in patients.

Project teams are currently working on further development and refinement, particularly the ultrasound rendering, the deformation of the organs and further transfer of training validation. Ultrasound rendering could be improved by incorporating the law of physics instead of only visual heuristics. Soft-tissue behavior could also be made more realistic by replacing the chainmail model by a more accurate model. Regarding validation, we are in the process of validating the simulator framework applied to nephrostomy, aiming to compare performance metrics from real procedures in order to show correlation between the performance in both

cases. Lastly, we are also exploring commercialisation of the completed simulator model.

Acknowledgements We would like to thank the late Roger Phillips for his significant contributions to the project. We acknowledge funding from the UK's Department of Health through the Health Technology Devices programme.

References

1. Bauer, C., Aurich, V., Arzhaeva, e.a.: Comparison and evaluation of methods for liver segmentation from CT datasets. *IEEE Transactions on Medical Imaging* **28**(8), 1251–1265 (2009)
2. Bottger, T., Kunert, T., Meinzer, H.P., Wolf, I.: Application of a new segmentation tool based on interactive simplex meshes to cardiac images and pulmonary MRI data. *Academic Radiology* **14**(3), 319–329 (2007)
3. Chi, Y., Cashman, P.M.M., Bello, F., Kitney, R.I.: A discussion on the evaluation of a new automatic liver volume segmentation method for specified CT image datasets. In: B. van Ginneken, T. Heimann, M. Styner (eds.) *Workshop on 3D Segmentation in the Clinic: A Grand Challenge*, pp. 167–175. *Med Image Comput Comput Assist Interv. MICCAI* (2007)
4. Coles, T.R., John, N.W., Gould, D.A., Caldwell, D.G.: Integrating haptics with augmented reality in a femoral palpation and needle insertion training simulation. *IEEE T. Haptics* **4**(3), 199–209 (2011)
5. Delorme, S., Laroche, D., DiRaddo, R., Del Maestro, R.F.: Neurotouch: a physics-based virtual simulator for cranial microneurosurgery training. *Neurosurgery* **71**(1 Suppl Operative), 32–42 (2012). DOI 10.1227/NEU.0b013e318249c744
6. Dillenseger, J.L., Laguitton, S., Delabrousse, E.: Fast simulation of ultrasound images from a ct volume. *Comp. in Bio. and Med.* **39**(2), 180–186 (2009)
7. Forest, C., Comas, O., Vaysière, C., Soler, L., Marescaux, J.: Ultrasound and needle insertion simulators built on real patient-based data. *Stud Health Technol Inform* **125**, 136–9 (2007)
8. Forest, C., Comas, O., Vaysière, C., Soler, L., Marescaux, J.: Ultrasound and needle insertion simulators built on real patient-based data. In: *Proceedings of MMVR 15*, pp. 136–139 (2007)
9. Fornage, B.: A simple phantom for training in ultrasound-guided needle biopsy using the freehand technique. *J Ultrasound Med.* **8**, 701–3 (1989)
10. van Gerwen, D.J., Dankelman, J., van den Dobbelsteen, J.J.: Needle-tissue interaction forces - a survey of experimental data. *Medical Engineering & Physics* (2012)
11. Gibson, S.F.: 3D chainmail: a fast algorithm for deforming volumetric objects. In: *Proc Symp on Interactive 3D Graphics*, pp. 149–154 (1997)
12. Hoppe, H., DeRose, T., Duchamp, T., McDonald, J., Stuetzle, W.: Surface reconstruction from unorganized points. In: *Computer Graphics (SIGGRAPH '92 proceedings)*, pp. 71–78 (1992)
13. Ibanez, L., Schroeder, W., Ng, L., Cates, J.: *The ITK Software Guide*. Kitware, Inc. ISBN 1-930934-15-7, <http://www.itk.org/ItkSoftwareGuide.pdf>, second edn. (2005)
14. Johnson, S., Hunt, C., Woolnough, H., Crawshaw, M., Kilkenny, C., Gould, D., Sinha, A., England, A., Villard, P.F.: Virtual reality, ultrasound-guided liver biopsy simulator: Development and performance discrimination. *British Journal of Radiology* (2011). DOI 10.1259/bjr/47436030
15. Karupphasamy, K., Zhai, J., How, T., Gould, D.: Development and validation of an unobtrusive sensor for in-vivo force data collection during interventional procedures. *Cardio-Vascular and Interventional Radiology* **32**, 22–23 (2008)
16. Li, Y., Brodli, K.: Soft object modelling with generalised chainmail - extending the boundaries of web-based graphics. *Comput. Graph. Forum* **22**(4), 717–728 (2003)
17. Lorensen, W.E., Cline, H.E.: Marching cubes: A high resolution 3D surface construction algorithm. *SIGGRAPH Comput. Graph.* **21**(4), 163–169 (1987). DOI 10.1145/37401.37422
18. Lovquist, E., O'Sullivan, O., Oh'Ainle, D., Baitson, G., Shorten, G., Avis, N.: Vr-based training and assessment in ultrasound-guided regional anesthesia: From error analysis to system design. In: *MMVR*, vol. 163, pp. 304–310. IOS Press (2011)

19. Magee, D., Zhu, Y., Ratnalingam, R., Gardner, P., Kessel, D.: An augmented reality simulator for ultrasound guided needle placement training. *Journal of Medical & Biological Engineering & Computing* **45**, 957–967 (2007)
20. Maurin, B., Barbé, L., Bayle, B., Zanne, P., Gangloff, J., de Mathelin, M., Soler, L., Forgione, A.: In vivo study of forces during needle insertions. In: *Proceedings of the Medical Robotics, Navigation and Visualisation Scientific Workshop 2004*. Germany, Remagen (2004)
21. McNamara Jr., M.P., McNamara, M.E.: Preparation of a homemade ultrasound biopsy phantom. *J Clin Ultrasound* **17**(6), 456–8 (1989)
22. Meier, U., López, O., Monserrat, C., Juan, M.C., Alcañiz, M.: Real-time deformable models for surgery simulation: a survey. *Comput. Methods Prog. Biomed.* **77**(3), 183–197 (2005)
23. Parikh, S.S., Chan, S., Agrawal, S.K., Hwang, P.H., Salisbury, C.M., Rafii, B.Y., Varma, G., Salisbury, K.J., Blevins, N.H.: Integration of patient-specific paranasal sinus computed tomographic data into a virtual surgical environment. *Am J Rhinol Allergy* **23**(4), 442–7 (2009). DOI 10.2500/ajra.2009.23.3335
24. Shams, R., Hartley, R., Navab, N.: Real-time simulation of medical ultrasound from CT images. *LNCS* **5242**, 734–741 (2008)
25. Stern, J., Zeltser, I.S., Pearle, M.S.: Percutaneous renal access simulators. *J Endourol* **21**(3), 270–3 (2007)
26. Tabriz, D.M., Street, M., Pilgram, T.K., Duncan, J.R.: Objective assessment of operator performance during ultrasound-guided procedures. *Int. J. Computer Assisted Radiology and Surgery* **6**(5), 641–652 (2011)
27. Vidal, F.P., John, N.W., Gould, D.A., Healey, A.E.: Simulation of ultrasound guided needle puncture using patient specific data with 3D textures and volume haptics. *Computer Animation and Virtual Worlds* **19**(2), 111–127 (2008). DOI 10.1002/cav.217
28. Vidal, F.P., Villard, P., Lutton, E.: Tuning of patient specific deformable models using an adaptive evolutionary optimization strategy. *IEEE Transactions on Biomedical Engineering* **59**(10), 2942 – 2949 (2012). DOI 10.1109/TBME.2012.2213251
29. Villard, P.F., Boshier, P., Bello, F., Gould, D.: Virtual Reality Simulation of Liver Biopsy with a Respiratory Component. In: H. Takahashi (ed.) *Liver Biopsy*. InTech (2011). URL <http://hal.inria.fr/inria-00621263>
30. Villard, P.F., Vidal, F.P., Hunt, C., Bello, F., John, N.W., Johnson, S., Gould, D.A.: A prototype percutaneous transhepatic cholangiography training simulator with real-time breathing motion. *Int J Comput Assist Radiol Surg* **4**(6), 571–578 (2009). DOI 10.1007/s11548-009-0367-1
31. Wahba, G.: *Spline models for observational data*, vol. 59. Society for industrial and applied mathematics (1990)
32. Willaert, W.I.M., Aggarwal, R., Van Herzeele, I., Cheshire, N.J., Vermassen, F.E.: Recent advancements in medical simulation: patient-specific virtual reality simulation. *World J Surg* **36**(7), 1703–12 (2012). DOI 10.1007/s00268-012-1489-0
33. Willaert, W.I.M., Aggarwal, R., Van Herzeele, I., Plessers, M., Stroobant, N., Nestel, D., Cheshire, N., Vermassen, F.: Role of patient-specific virtual reality rehearsal in carotid artery stenting. *Br J Surg* **99**(9), 1304–13 (2012). DOI 10.1002/bjs.8858
34. Wilson, T.A., Legrand, A., Gevenois, P.A., De Troyer, A.: Respiratory effects of the external and internal intercostal muscles in humans. *Journal of Physiology* **530**(2), 319–330 (2001)
35. Yushkevich, P.A., Piven, J., Cody Hazlett, H., Gimpel Smith, R., Ho, S., Gee, J.C., Gerig, G.: User-guided 3D active contour segmentation of anatomical structures: Significantly improved efficiency and reliability. *Neuroimage* **31**(3), 1116–1128 (2006)